Available online at www.sciencedirect.com
ScienceDirect
International Journal of Mass Spectrometry 264 (2007) 22–37
International Journal of Mass Spectrometry
www.elsevier.com/locate/ijms

Temporary anion states and dissociative electron attachment to nitrobenzene derivatives

N.L. Asfandiarov [a,*], S.A. Pshenichnyuk [a], V.G. Lukin [a], I.A. Pshenichnyuk [b], A. Modelli [c,d], Š. Matejčik [e]

[a] *Institute of Physics of Molecules and Crystals, Ufa Research Center of RAS, October Prospect, 151, Ufa 450075, Russia*
[b] *Charles University, Institute of Theoretical Physics, V Holesovickach 2, 18000 Prague, Czech Republic*
[c] *Dipartimento di Chimica "G. Ciamician", Università di Bologna, Via Selmi 2, 40126 Bologna, Italy*
[d] *Centro Interdipartimentale di Ricerca in Scienze Ambientali, Università di Bologna, via S. Alberto 163, 48100 Ravenna, Italy*
[e] *Department of Experimental Physics, Comenius University, Mlynska dolina F2, 84248 Bratislava, Slovak Republic*

Received 21 February 2007; received in revised form 20 March 2007; accepted 20 March 2007
Available online 27 March 2007

Abstract

The nitrobenzene derivatives 1,2-nitrotoluene, 1,3-nitrotoluene, 1,2-fluoronitrobenzene, 1,3-fluoronitrobenzene, 1,4-fluoronitrobenzene, 1,2-chloronitrobenzene, 1,3-chloronitrobenzene and 1,4-chloronitrobenzene are investigated by means of electron transmission spectroscopy (ETS), dissociative electron attachment spectroscopy (DEAS) and negative ion mass spectrometry (NIMS). The observed energies of electron attachment to π* MOs were interpreted with the support of the empty level structures of the neutral molecules supplied by HF/6-31G and B3LYP/6-31G* calculations. In the chlorine-substituted derivatives three main long-lived negative ions (NIs) (M^-, Cl^-, and NO_2^-) are observed, only M^- and NO_2^- in the other investigated compounds. The detection of the metastable NIs corresponding to the process $M^{*-} \rightarrow R^- + (M–R)^\bullet$ suggests that the molecular NIs formed near thermal electron energy dissociate on a microsecond timescale. Mean autodetachment lifetimes of the molecular NIs as a function of electron energy are evaluated.

Keywords: Dissociative electron attachment; ETS; DEAS

1. Introduction

Electron transmission spectroscopy (ETS) [1,2] is one of the most suitable means for measuring the energies of formation of unstable anion states in the gas-phase. This technique takes advantage of the sharp variations in the total electron–molecule scattering cross section caused by resonance processes, namely, temporary capture of electrons with appropriate energy and angular momentum into empty molecular orbitals (MOs) [3]. The electron attachment process is rapid with respect to the nuclear motion, so that the temporary anions are formed in the equilibrium geometry of the neutral molecule. The measured vertical attachment energies (VAEs) represent the negative values of the vertical electron affinities (EAs).

Additional information on negative ion formation can be supplied by dissociative electron attachment spectroscopy (DEAS) [2] which measures the yield of long-lived negative ions, as a function of the impact electron energy. When suitable energetic and kinetic conditions occur, the temporary molecular anions observed in ETS can follow a dissociative decay channel before the extra electron is re-emitted. The lifetime of the negative fragments produced is usually sufficiently long to allow detection by means of a mass filter.

Because of the strong inductive effect and the low energy of the lowest unoccupied MO (LUMO) of the NO_2 functional group, nitro derivatives possess very pronounced electron-acceptor properties. From the point of view of the reactivity, the knowledge of the empty level structure is even more important than that of the filled counterpart. Nevertheless, to our knowledge the ETS literature is limited to a work on the reactivity of a large conjugated π-system [4] and to a study of nitrobenzene and its hydroxy and methoxy derivatives [5], where the energy trends of the observed VAEs were reproduced by the empty MO

* Corresponding author. Tel.: +7 347 2313538; fax: +7 347 2313538.
E-mail address: nail@anrb.ru (N.L. Asfandiarov).

1387-3806/$ – see front matter © 2007 Elsevier B.V. All rights reserved.
doi:10.1016/j.ijms.2007.03.013

energies supplied by Hartree–Fock (HF) calculations using the 6-31G* and D95V* basis sets, which do not include diffuse functions.

A theoretical description of the unstable anion states presents difficulties. A proper description of such spatially diffuse species, in fact, would require a basis set with diffuse functions. However, as the basis set is expanded, an SCF calculation ultimately describes a neutral molecule and an unbound electron in the continuum, and generates low-energy solutions having no physical significance with regard to anion formation [6,7]. In addition, the calculated energies depend upon the basis set choice; so that it is a hard task to decide a priori which basis set (if any) will be reliable for reproducing the energies of unstable anion states [8]. However, Staley and Strnad [6] and Chen and Gallup [9] demonstrated that the π^*_{CC} VAEs measured in ETS are linearly correlated with the corresponding HF virtual orbital energies (VOEs) of the neutral molecules, calculated with basis sets which do not include diffuse functions, and that this simple computational approach can be used for quantitative prediction of π^* VAEs in unsaturated hydrocarbons. More recently, an analogous good linear correlation has also been found [7] with the VOEs supplied by B3LYP/6-31G* calculations.

An electron–molecule collision leading to the dissociation of a temporary anion state is the simplest example of an electron-transfer induced chemical reaction:

$$AB + e^- \rightarrow AB^{*-} \rightarrow A^- + B,$$

where AB is a target molecule. Such processes play an important role in many different research areas such as low-temperature plasma physics, chemistry, biochemistry, and environmental sciences, among others. The electron–target interaction as well as the ensuing chemical reaction can, in general, depend on the molecular environment. Nevertheless, the gas-phase properties of the molecule (such as EA, total scattering and DEA cross sections) remain of fundamental significance, shaping its behavior in any aggregate state. However, a model of these processes with predictive power has not yet been developed. DEAS and NIMS, closely connected with the ETS technique [5,10], give information on the dissociative decay channels which follow electron attachment. The DEA cross section $\sigma_{DA}(E)$ may be represented as the product of a capture cross section $\sigma_{Cap}(E)$ and the anion survival factor ρ [10,11], where E is the electron impact energy:

$$\sigma_{DA}(E) = \sigma_{Cap}(E)\rho. \quad (1)$$

DEAS information on nitrobenzene derivatives [5,12,13] is rather scarce, although in the 1970s Christophorou et al. [14] measured the lifetime of the parent anion formed at zero energy in a variety of nitrobenzene derivatives and elaborated a semi-empirical theory for the autodetachment decay of parent negative ions [15]. This approach, however, requires knowledge of the electron attachment cross section. A recent NIMS study [16] of 25 nitrobenzens explored the suitability of this technique as a tool for molecular identification of electrophilic compounds.

Here we report for the first time the ET spectra of methyl, fluoro and chloro derivatives of nitrobenzene. The assignment of the spectral features to the corresponding anion states is supported by comparison between the measured VAEs and those obtained by scaling the HF/6-31G and B3LYP/6-31G* VOEs of the neutral state molecules with empirical linear equations available in the literature [5,6]. The same equations also allow to evaluate the positive EAs associated with formation of stable anion states, which cannot be observed in ETS.

The DEA spectra of the same compounds are also presented, to get insight into the dissociative decay channels of the various resonances, the nature of the negative fragments produced and their relative abundance.

2. Experiment

In NIMS experiment an electron beam passes through the ionization chamber of a mass spectrometer filled with the gas-phase molecules under investigation. The negative ions formed are recorded mass spectrometrically as a function of the incident electron energy. The mass spectrometer consists of a negative ion source, 90° magnetic sector analyzer, and secondary electron multiplier with a multiplication factor of about 10^6. The vacuum system is heatable up to 300 °C and consists of two 100 l/s oil diffusion pumps with liquid nitrogen traps. One pump is used for evacuating the chamber in which the negative ion source is located. The other one reduces the pressure in the chamber where the secondary electron multiplier is placed. The residual pressure in the vacuum system of the mass spectrometer does not exceed 1.5×10^{-8} Torr.

All electrodes of the negative ion source are made of stainless steel and coated with soot, in order to reduce the reflection of electrons from the electrodes. The coating also decreases the formation of dielectric films on electrode surfaces, which may influence the electric potentials inside the anion source. The electrons emitted from a tungsten filament are collimated by an axial magnetic field of about 80 G. The electrons with an energy distribution of about 0.4 eV are accelerated into the collision chamber where they interact with the target gas. The pressure inside the collision chamber is kept as low as $\sim 10^{-6}$ Torr in order to ensure single-collision conditions. After passing the collision chamber, the electrons are collected by an electron trap. The electron current is about 1 μA at the electron energy of 8 eV. The full electron energy range accessible in this experiment was 0–12 eV. Negative ions are extracted from the collision chamber and accelerated to the magnetic mass analyzer by a potential difference of 4 kV. The time of flight for the SF_6^- ion (m/z 146), from its formation in the negative ion source to detection with the secondary electron multiplier, is about 20 μs. Scanning of the electron energy and the mass number is carried out by an IBM-comparable computer using a CAMAC interface, with an energy step of 16 meV. The estimated accuracy of determination of the peak positions is ±0.1 eV.

The electron energy scale is calibrated with reference to the SF_6^- anion from SF_6 which gives the well-known resonance peak at 0 eV. The natural shape of this resonance may be approximately fitted by a δ-function, the full width at half maximum (FWHM) being extremely small [8]. Thus, the measured width of the SF_6^- ion reflects the electron energy distribution in the ion source. The relatively poor energy resolution (FWHM

~0.4 eV), in comparison for example with tens of meV in an apparatus equipped with a trochoidal electron monochromator [9], however, allows to detect low-intensity signals. In addition, the sensitivity can be further enhanced by accumulating the signals obtained in different electron energy scans.

In contrast to quadruple or time-of-flight mass filters, the magnetic mass filter possesses an important advantage, namely, the possibility to detect the so called metastable NI [17]. These ions form outside the ionization camber of the ion source on the time scale of 1–10 μs, depending on the repulsive potential in the ion source. Registration of metastable NIs is a direct experimental evidence for the occurrence of very slow dissociation processes.

The ET spectra were measured at the University of Bologna using an apparatus in the format devised by Sanche and Schulz [1], and previously described [18]. The present spectra were obtained in the "high rejection" mode [19], and are therefore related to the nearly total scattering cross-section. The electron beam resolution was about 50 meV (FWHM). The energy scale was calibrated with reference to the $(1s^1 2s^2)^2S$ anion state of He. The estimated accuracy of the measured VAEs is ±0.05 eV.

High-resolution (FWHM = 100 meV) DEA spectra were measured at the Comenius University, Bratislava, with an apparatus described in details elsewhere [20].

All compounds are commercially available from Sigma–Aldrich Inc.

2.1. Computational details

Geometry optimisations and evaluation of the virtual orbital energies of the neutral molecules were obtained at the HF/6-31G and B3LYP/6-31G* levels. The first vertical and adiabatic EAs of nitrobenzene and 4-F-nitrobenzene were computed as the total energy difference between the neutral and anion states (the latter with the optimized geometry of the neutral state or with its optimized geometry, respectively) at the B3LYP/6-31 + G* level. The calculations were performed with the Gaussian 98 set of programs [21]. Statistical model calculations were performed using Maple 8.0 by Waterloo Maple Inc.

3. Results

3.1. ET spectra

The ET spectra of the nitrobenzene derivatives NO_2–C_6H_4–X, with X = CH_3, F and Cl, are presented in the upper left panels of Figs. 1–8. The vertical lines locate the measured VAEs, given in Table 1. In all compounds, the first anion state is stable (thus not observed in ETS). The experimental adiabatic EAs, however, are available in the literature [22–24]. Although the adiabatic EAs are associated with the anion in its optimized geometry, their values (with negative sign) are reported in Table 1 in the column of the experimental VAEs.

The assignment of the ET spectral features to the corresponding MOs can be based on that previously reported [5] for nitrobenzene. Nitrobenzene (C_{2v} point group) has four empty π* orbitals. The LUMO, with mainly π* NO_2 character and mixed with the component of b_1 symmetry of the degenerate benzene π* (e_{2u}) MO, gives rise to a stable anion state. The first resonance displayed (at 0.55 eV) by the ET spectrum is associated with the non-interacting ring π* (a_2) component of the benzene π* (e_{2u}) LUMO, inductively stabilized (about 0.6 eV with respect to benzene [18]) by the electron-withdrawing nitro group. The second resonance of the spectrum (1.36 eV) is due

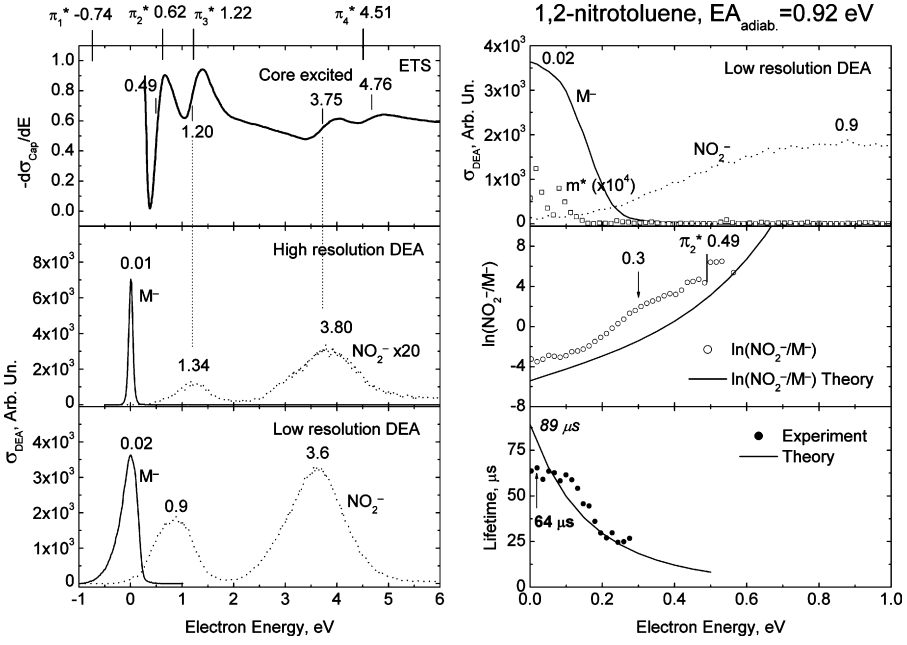

Fig. 1. Left panels: ETS (~300 K, vertical lines indicate the VAEs), DEA with high-electron energy resolution (~300 K) and NIMS with high-sensitivity (~350 K) data for 1,2-nitrotoluene. Right panel: enlarged low-energy region of the low-resolution DEA spectrum including metastable NIs (upper panel); experimental and calculated decay curves for 1,2-nitrotoluene; the arrow indicates a change of slope of the experimental decay curve (middle panel); mean autodetachment lifetime of the molecular NI as a function of energy and theoretical extrapolation to zero electron energy (bottom panel).

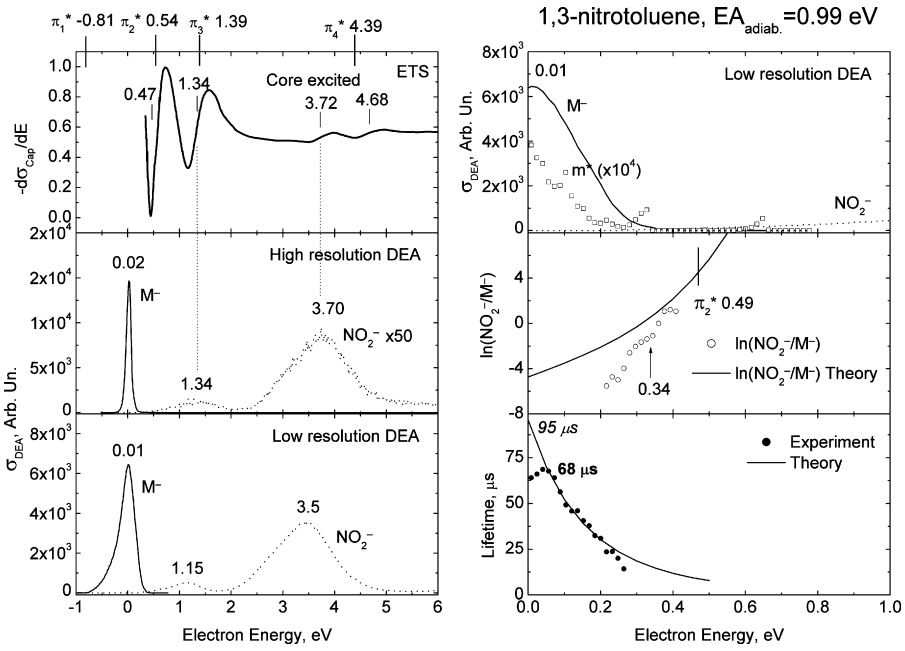

Fig. 2. As in Fig. 1 for 1,3-nitrotoluene.

to the b_1 component of the benzene LUMO, mixed in an antibonding manner with the π* NO_2 MO. Electron capture into the highest-lying empty π* (b_1) MO (with mainly totally antibonding benzene π* (b_{2g}) character, VAE = 4.82 eV in benzene [18]) is associated with the resonance at 4.69 eV, the remaining resonance (at 3.79 eV) being ascribed [5] to a core-excited shape resonance, that is, electron capture accompanied by a valence electron excitation.

As mentioned above, it was shown that the experimental π* VAEs of unsaturated hydrocarbons are linearly correlated to the corresponding VOEs of the neutral molecules, and that this simple approach can be used for their quantitative prediction. Table 1 reports the VOEs obtained with HF/6-31G and B3LYP/6-31G* calculations and (in parentheses) the VAEs predicted by the appropriate linear scaling given in Refs. [6,7], respectively, for the HF and B3LYP calculations. The VAEs obtained from the HF/6-31G VOEs are also represented as vertical lines above each ET spectrum in Figs. 1–8.

The energies of the first two resonances (associated with the second and third anion states) displayed in the ET spectrum of nitrobenzene are nicely reproduced (within ±0.1 eV) by both the HF/6-31G and B3LYP/6-31G* scaled VOEs (see Table 1). The VAE of the higher lying π* (b_1) MO is somewhat underestimated, especially with the B3LYP calculations. However, this

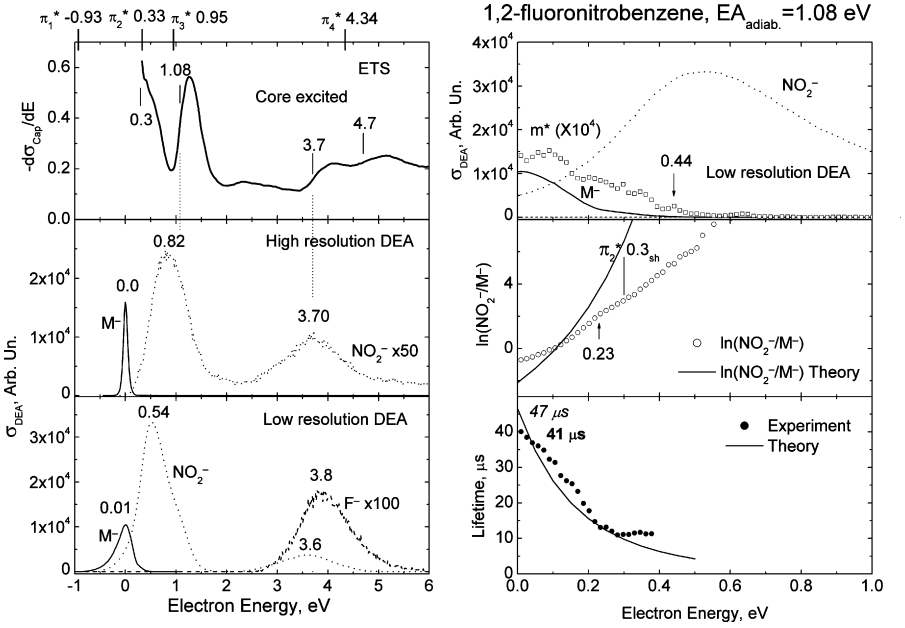

Fig. 3. As in Fig. 1 for 1,2-fluoronitrobenzene.

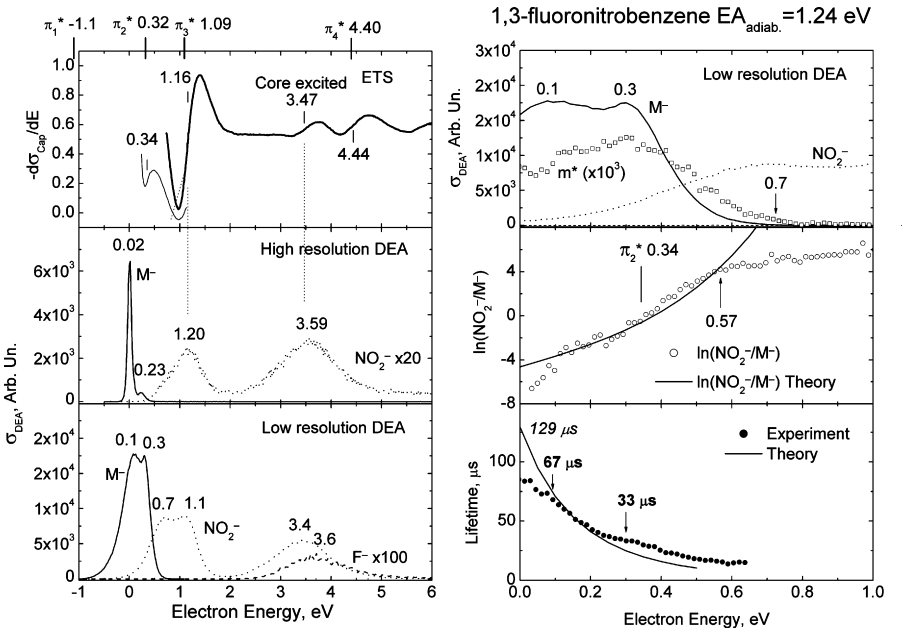

Fig. 4. As in Fig. 1 for 1,3-fluoronitrobenzene.

is to be expected because this resonance is likely destabilized by mixing with the (close in energy) core-excited resonance located at 3.79 eV. This interaction, of course, is not accounted for by the neutral state calculations. Finally, the scaled VOEs predict the first vertical π* anion of nitrobenzene to be sizeably stable (about 0.8 eV, see Table 1), in nice agreement with a 0.2 eV larger experimental adiabatic EA (1.01 eV [22]). The geometrically relaxed anion, in fact, is more stable than the vertical anion.

In order to get a more quantitative assessment of their difference in this class of compounds, we have calculated the first vertical and adiabatic EAs of nitrobenzene and 4-F-nitrobenzene as the energy difference between the neutral and anion states at the B3LYP/6-31 + G* level (i.e., using a basis set which includes the minimum addition of diffuse functions). The following vertical and adiabatic, respectively, EA values have been obtained: nitrobenzene 0.890 eV, 1.199 eV; 4-F-nitrobenzene 0.993 eV, 1.314 eV. For both the vertical and the optimized anions, the singly occupied MO is correctly predicted to be a valence MO of π b_1 symmetry. The adiabatic EA, slightly (0.2 eV) overestimated with respect to experiment, is calculated to be 0.3 eV larger than the vertical EA. For all the nitrobenzenes considered, 0.3 eV is just the difference between the experimental adiabatic EA and the vertical EA supplied by the scaled B3LYP VOEs (see Table 1), thus indicating the reliability of the latter values.

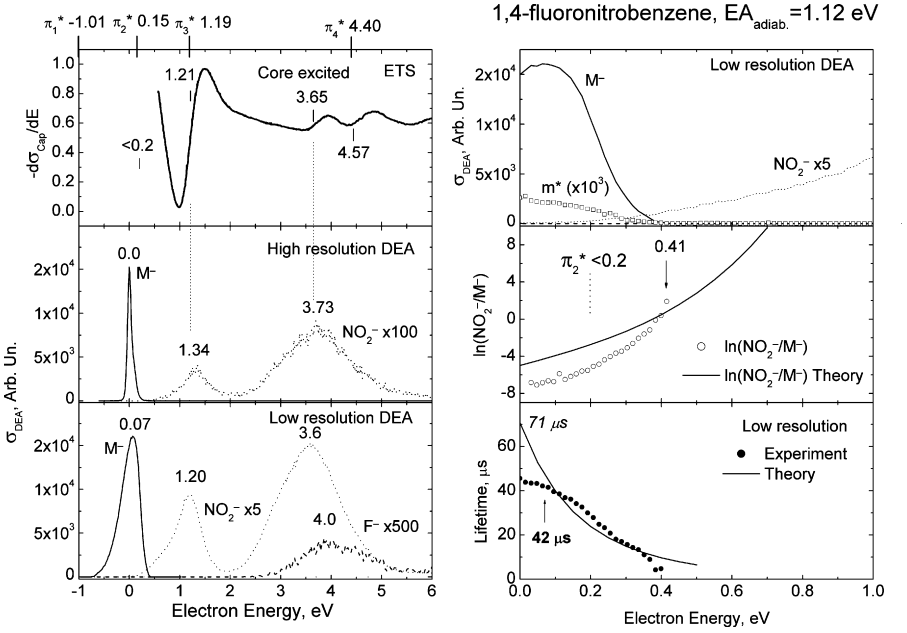

Fig. 5. As in Fig. 1 for 1,4-fluoronitrobenzene.

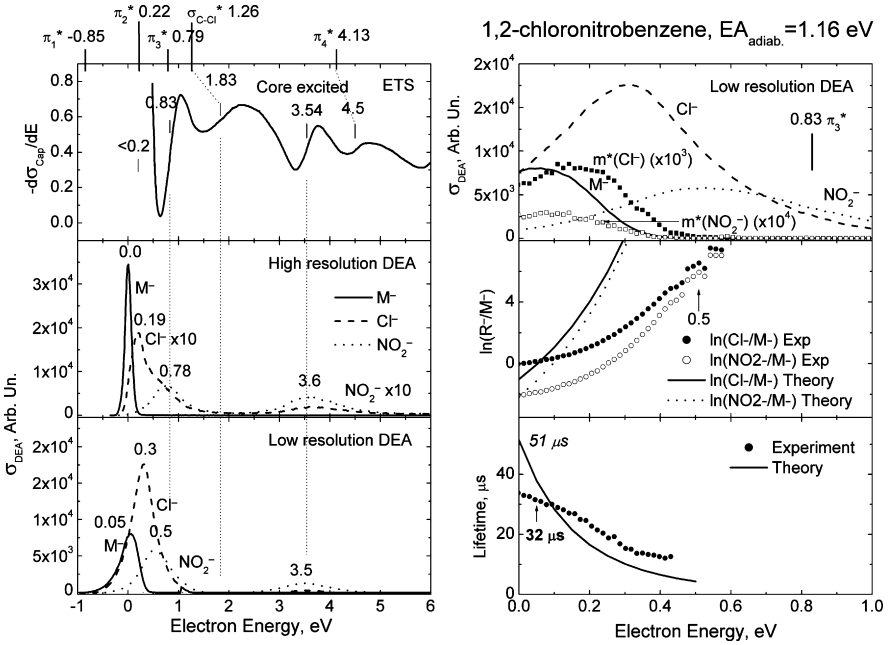

Fig. 6. As in Fig. 1 for 1,2-chloronitrobenzene.

Literature ET data [18,23] showed that methyl substitution on the benzene ring causes only small energy perturbations of the π* anion states. In agreement, the ET spectrum of 3-methyl-nitrobenzene looks very similar to that of nitrobenzene. Its VAEs, as well as the adiabatic EA, are close to those of the unsubstituted compound. In 2-methyl-nitrobenzene, because of steric hindrance caused by ortho substitution, the conformation where the NO_2 group is somewhat rotated out of the ring plane (dihedral angle = 13.23°, according to the B3LYP/6-31G* calculations) is slightly more stable than the coplanar conformer. Consistently, due to the smaller $\pi^*_{NO_2}/\pi^*_{ring}$ interaction, the energies (experimental and calculated) of the first and third anion states are about 0.1 eV higher and smaller, respectively, with respect to 3-methyl-nitrobenzene. As far as the highest-lying benzene π* MO is concerned, it is to be noticed that in the methyl derivatives both the HF and B3LYP calculations predict the presence of two MOs with similar nature (localized on the ring and the CH_3 group). The energy reported in Table 1 is an average value.

The main effect produced by fluorine and chlorine substitution is an inductive stabilization of all the π* anion states. Because of this shift to lower energy, the ring a_2 resonance

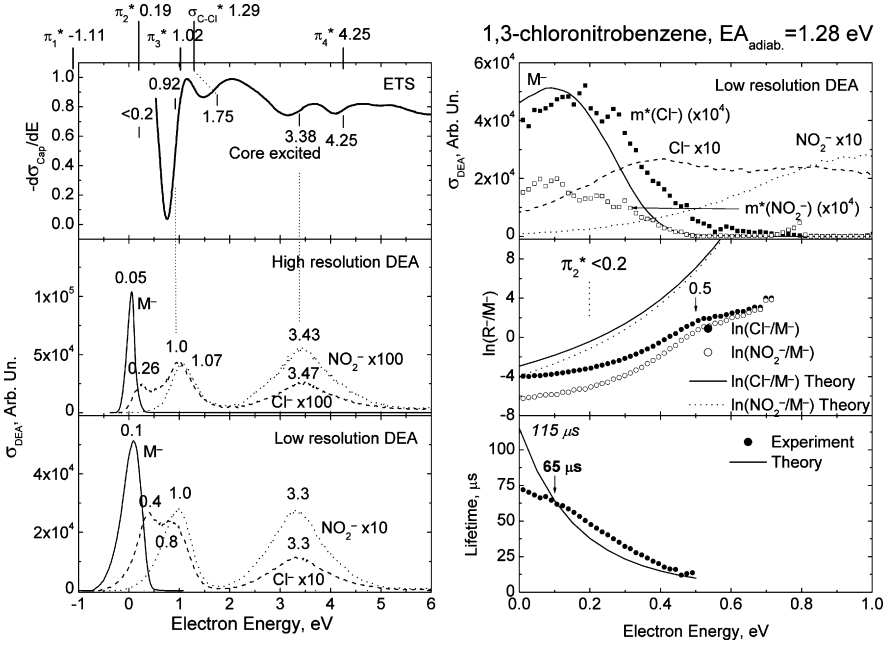

Fig. 7. As in Fig. 1 for 1,3-chloronitrobenzene.

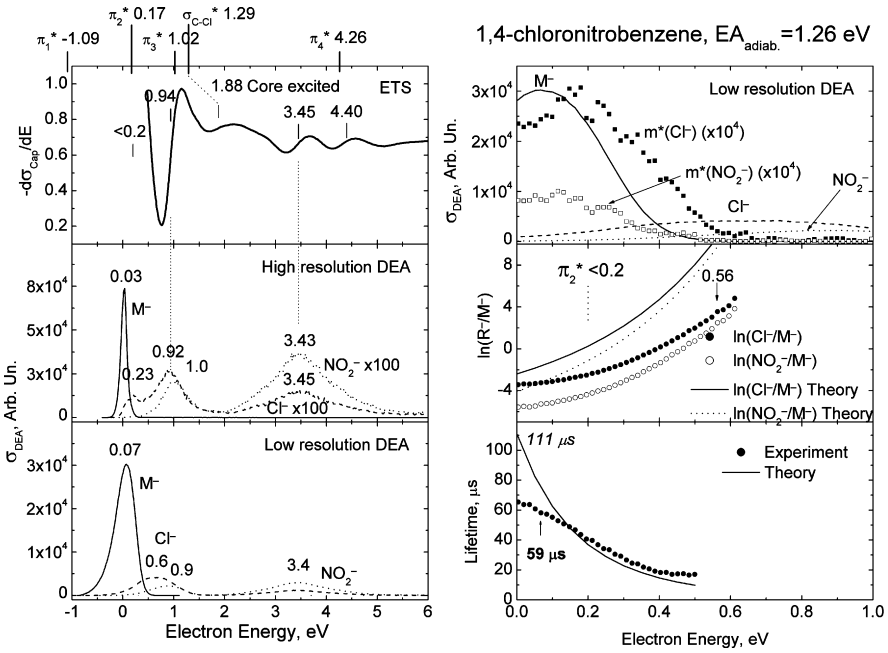

Fig. 8. As in Fig. 1 for 1,4-chloronitrobenzene.

appears as a shoulder on the high-energy side of the intense electron beam signal at zero energy, in some cases being completely masked.

Also for the 2-halo derivatives the calculations predict a rotated conformer to be slightly more stable than the planar conformer. According to the B3LYP calculations, the dihedral angle between the NO_2 and ring planes is 12.81° in 2-fluoro-nitrobenzene and 33.34° in 2-chloro-nitrobenzene. As already observed for 2-nitrotoluene, in 2-fluoro- and 2-chloro-nitrobenzene the energy gap between the first and third anion states is smaller than that of the corresponding coplanar *meta* and *para* isomers.

As expected [23], in the chloro derivatives the presence of a third-row element causes the occurrence of an additional low-energy resonance, associated with electron capture into a σ^*_{C-Cl} MO. This resonance, located at 2.42 eV in chlorobenzene [23], is centered around 1.8 eV in all three chloronitrobenzenes, in line with the electron-withdrawing effect of the nitro group. Table 1 reports the scaled VOEs also for the σ^*_{C-Cl} MOs, although the empirical linear correlations employed were calibrated only with π* VAEs. In fact, the agreement between the scaled σ* VOEs and the corresponding measured VAEs is worse than that found for the π* VAEs.

3.2. High-resolution DEA spectra

The relative DEA cross sections as a function of incident electron energy, the so-called curves of effective ion yield (CEIY), measured with high-electron energy resolution (FWHM ∼ 100 meV) at room temperature ($T \sim 300$ K) are shown in the central left panels of Figs. 1–8. In the chloro derivatives two dominant decay channels of the temporary parent NIs are observed, corresponding to formation of Cl^- and NO_2^- fragments. Long-lived parent NIs (M^-) were also found. These results are in agreement within an order of magnitude with earlier data [13,14]. The intensity of F^- fragments anions in the spectra of the fluoro derivatives was too small (if any) to be detected. Thus, in the fluoro and methyl derivatives only the CEIYs for M^- and NO_2^- have been recorded. The peak of the M^- current is observed at thermal electron energy in all compounds under investigation. As previously suggested [15], these signals are likely associated with vibrational Feshbach resonances.

As noted above, electron attachment to the empty π^*_2 MO leads to formation of the ring shape resonance of $^2A_2$ symmetry (in the C_{2v} point group notation). In the ET spectra of the chloro derivatives the corresponding feature is masked by the intense electron beam signal. In 1,2-fluoronitrobenzene this resonance appears as a shoulder at 0.3 eV (Fig. 3), while it is clearly seen in nitrobenzene at 0.55 eV [5], its methyl derivatives (Figs. 1 and 2) at 0.49 and 0.47 eV, respectively, and in 1,3-fluoronitrobenzene (Fig. 4) at 0.34 eV. In the DEA spectrum of 1,3-fluoronitrobenzene the M^- current displays a distinct peak at 0.23 eV, which may be assigned to formation of the π^*_2 anion state. The intensity of this signal is several times larger than that of the NO_2^- current (Table 2). In contrast, the corresponding resonant state in *o*-, *m*-, and *p*-chloronitrobenzene mainly follows the DEA channel, which leads to formation of Cl^- fragment anions. This process is forbidden by symmetry reasons in the rigid planar conformation of the neutral state, and relies upon vibronic coupling under out-of-plane vibration of the halogen atom, which reduces the anion symmetry [25].

Figs. 1–8 show the energy correspondence between the maxima of the NO_2^- (and Cl^- in the chloro derivatives) currents in the high-resolution DEA spectra and the π^*_3 temporary negative ion states observed in ET spectra around 1 eV. These dissociation channels are also forbidden by symmetry. Also the signals observed at ∼3.6 eV in the ET spectra (assigned to core excited

Table 1
Calculated virtual orbital energies (VOEs) and corresponding scaled values (VAEs) in parentheses (see text)

NO_2–C_6H_4–X	Orbital (C_{2v} notation)	VOE (VAE) HF/6-31G	VOE (VAE) B3LYP/6-31G*	Experimental VAE (FWHM) (eV)
H[a]	π^* b_1 (ring)	9.255 (4.56)	3.844 (4.31)	4.69 (0.50), $3.79_{\text{core excited}}$ (0.50)
	π^* b_1 (ring–NO_2)	4.261 (1.30)	0.016 (1.22)	1.36 (0.40)
	π^* a_2 (ring)	3.032 (0.50)	−0.753 (0.60)	0.55 (0.35)
	π^* b_1 (NO_2 + ring)	0.954 (−0.86)	−2.430 (−0.75)	−1.01 ± 0.10 (adiab.)[b]
2-CH_3	π_4^* b_1 (ring)	9.176 (4.51)[c]	4.388 (4.75)[c]	4.76 (0.58), $3.75_{\text{core excited}}$ (0.58)
	π_3^* b_1 (ring–NO_2)	4.130 (1.22)	−0.012 (1.20)	1.20 (0.37)
	π_2^* a_2 (ring)	3.222 (0.62)	−0.596 (0.73)	0.49 (0.31)
	π^* b_1 (NO_2 + ring)	1.135 (−0.74)	−2.308 (−0.65)	−0.92 ± 0.10 (adiab.)[b]
3-CH_3	π_4^* b_1 (ring)	9.038 (4.39)[c]	4.258 (4.65)[c]	4.68 (0.60), $3.72_{\text{core excited}}$ (0.51)
	π_3^* b_1 (ring–NO_2)	4.397 (1.39)	0.143 (1.33)	1.34 (0.40)
	π_2^* a_2 (ring)	3.089 (0.54)	−0.690 (0.66)	0.47 (0.34)
	π^* b_1 (NO_2 + ring)	1.033 (−0.81)	−2.349 (−0.68)	−0.99 ± 0.10 (adiab.)[b]
2-F	π^* b_1 (ring)	8.917 (4.34)	3.719 (4.21)	4.7 (0.66), $3.70_{\text{core excited}}$ (0.75)
	π^* b_1 (ring–NO_2)	3.716 (0.95)	−0.221 (1.03)	1.08 (0.37)
	π^* a_2 (ring)	2.777 (0.33)	−0.811 (0.56)	0.3_{sh}
	π^* b_1 (NO_2 + ring)	0.837 (−0.93)	−2.495 (−0.80)	−1.08 ± 0.10 (adiab.)[b]
3-F	π^* b_1 (ring)	9.012 (4.40)	3.727 (4.21)	4.44 (0.56), $3.47_{\text{core excited}}$ (0.44)
	π^* b_1 (ring–NO_2)	3.937 (1.09)	−0.137 (1.10)	1.16 (0.41)
	π^* a_2 (ring)	2.757 (0.32)	−0.841 (0.53)	0.34 (0.17)
	π^* b_1 NO_2 + ring)	0.570 (−1.10)	−2.640 (−0.92)	−1.24 ± 0.10 (adiab.)[b]
4-F	π^* b_1 (ring)	9.008 (4.40)	3.719 (4.21)	4.57 (0.51), $3.65_{\text{core excited}}$ (0.52)
	π^* b_1 (ring–NO_2)	4.068 (1.19)	−0.008 (1.20)	1.21 (0.5)
	π^* a_2 (ring)	2.502 (0.15)	−1.072 (0.35)	≤0.2
	π^* b_1 (NO_2 + ring)	0.720 (−1.01)	−2.501 (−0.80)	−1.12 ± 0.10 (adiab.)[b]
2-Cl	π^* b_1 (ring)	8.598 (4.13)	3.391 (3.94)	4.5 (0.7), $3.54_{\text{core excited}}$ (0.48)
	π^*_{C-Cl}	4.195 (1.26)	0.251 (1.41)	1.83 (0.83)
	π^* b_1 (ring–NO_2)	3.477 (0.79)	−0.490 (0.82)	0.83 (0.4)
	π^* a_2 (ring)	2.603 (0.22)	−1.053 (0.36)	≤0.2
	π^* b_1 (NO_2 + ring)	0.957 (−0.85)	−2.481 (−0.79)	−1.16 ± 0.10 (adiab.)[b]
3-Cl	π^* b_1 (ring)	8.744 (4.25)	3.424 (3.97)	4.25 (0.47), $3.38_{\text{core excited}}$ (0.50)
	π^*_{C-Cl}	4.240 (1.29)	0.229 (1.40)	1.75 (0.57)
	π^* b_1 (ring–NO_2)	3.831 (1.02)	−0.324 (0.95)	0.92 (0.43)
	π^* a_2 (ring)	2.552 (0.19)	−1.108 (0.32)	≤0.2
	π^* b_1 (NO_2 + ring)	0.573 (−1.11)	−2.704 (−0.97)	−1.28 ± 0.10 (adiab.)[b]
4-Cl	π^* b_1 (ring)	8.787 (4.26)	3.432 (3.98)	4.40 (0.45), $3.45_{\text{core excited}}$ (0.50)
	π^*_{C-Cl}	4.242 (1.29)	0.232 (1.40)	1.88 (0.45)
	π^* b_1 (ring–NO_2)	3.831 (1.02)	−0.329 (0.95)	0.94 (0.47)
	π^* a_2 (ring)	2.528 (0.17)	−1.130 (0.30)	≤0.2
	π^* b_1 (NO_2 + ring)	0.529 (−1.09)	−2.667 (−0.94)	−1.26 ± 0.10 (adiab.)[b]

Experimental VAEs and FWHM (in parentheses) are also reported. All values in eV.
[a] ETS data from Ref. [4].
[b] Negative of the experimental adiabatic EA [22].
[c] Average energy of two MOs localized on the ring and the CH_3 substituent.

anion states) have corresponding counterparts in the DEA spectra. Analogous correlations were previously found in the ET and DEA spectra of nitrobenzene [5].

No signals around 1.8 eV, where the ET spectra show a distinct σ^*_{C-Cl} resonance, are detected in the DEA spectra of the chloro nitrobenzenes, as well as in that of chlorobenzene [26]. In the ET spectrum of the latter, the σ^*_{C-Cl} anion state is located at 2.44 eV, whereas the DEA spectrum displays a maximum in the Cl^- current at 0.75 eV, i.e., very close in energy to the nearly degenerate $^2A_2$ and $^2B_1$ (π_2^* and π_3^*) anion states [26]. The Cl^- maximum observed around 0.2 eV in the DEA spectra of the chloro nitrobenzenes is thus reasonably associated with the corresponding $^2A_2$ (π_2^*) anion states, too close to zero energy to be detected in the ET spectra.

Aflatooni and Burrow [27] found the following relationship between the σ^*_{C-Cl} VAEs and the widths of the resonances observed in the ET spectra of polychloroalkanes: $\Delta E_{dps} = 0.51 VAE^{1.44}$, where ΔE_{dps} is the deep-to-peak energy separation in the derivatised signal. In agreement with the expected p_σ character of σ^*_{C-Cl} MOs, the Wigner threshold law ($\Gamma \propto E^{\ell+1/2}$) [28] with $\ell = 1$ predicts the same dependence of the average autodetachment width (Γ) on energy. Typical

Table 2
DEAS data on halonitrobenzenes at room temperature (~300 K)

m/z	E_{max} (FWHM) (eV)	Relative intensity (% in parentheses)	Integral intensity including all, isotopes (%)	Structure
1,2-Nitrotoluene				
137	0.01 (0.096)	7,041 (96.9)	72.9	M^-
46	1.34 (0.66)	60 (0.8)	4.6	NO_2^-
	3.80 (1.3)	165 (2.3)	22.5	
1,3-Nitrotoluene				
137	0.02 (0.112)	14,660 (98.6)	87.6	M^-
46	1.34 (0.7)	30 (0.2)	1.1	NO_2^-
	3.70 (1.3)	180 (1.2)	11.3	
1,2-Fluoronitrobenzene				
141	0.0 (0.096)	15,950 (95.8)	72	M^-
46	0.82 (0.84)	490 (2.9)	16.7	NO_2^-
	3.70 (1.4)	205 (1.2)	11.3	
1,3-Fluoronitrobenzene				
141	0.02 (0.097)	6,457 (89.5)	65.9	M^-
	0.23 (~$0.2_{est.}$)	426 (5.9)	6.4	
46	1.2 (0.72)	124 (1.7)	8.5	NO_2^-
	3.59 (1.3)	205 (2.8)	19.2	
1,4-Fluoronitrobenzene				
141	0.0 (0.097)	15,248 (99.2)	92.5	M^-
46	1.34 (0.5)	36 (0.2)	1.2	NO_2^-
	3.73 (1.46)	86 (0.6)	6.3	
1,2-Chloronitrobenzene				
157	0.0 (0.128)	35,276 (91.7)	72.3	M^-
46	0.78 (0.64)	704 (1.8)	5.0	NO_2^-
	3.6 (1.12)	430 (1.1)	5.1	
35	0.19 (~$0.4_{est.}$)	1,878 (4.9)	14.1	Cl^-
	3.73 (1.36)	197 (0.5)	3.5	
1,3-Chloronitrobenzene				
157	0.05 (0.128)	103,916 (98.2)	92.9	M^-
46	1.07 (0.54)	432 (0.4)	0.9	NO_2^-
	3.43 (1.26)	562 (0.5)	2.7	
35	0.26 (~$0.4_{est.}$)	250 (0.2)	0.4	Cl^-
	1.0 (0.6)	444 (0.4)	1.4	
	3.47 (1.35)	265 (0.3)	1.8	
1,4-Chloronitrobenzene				
157	0.03 (0.129)	73,720 (98.5)	90.7	M^-
46	1.0 (0.55)	208 (0.3)	1.1	NO_2^-
	3.43 (1.32)	367 (0.5)	4.4	
35	0.23 (~$0.4_{est.}$)	129 (0.2)	0.3	Cl^-
	0.92 (0.59)	266 (0.4)	1.6	
	3.45 (1.37)	154 (0.2)	1.9	

σ^*_{C-Cl} VAEs in monosubstituted chloroalkanes range from 1.8 to 3.45 eV [27]. The present chloronitrobenzenes exhibit comparable σ^*_{C-Cl} VAEs. Therefore the same magnitude of DEA cross section (~10^{-18} to 10^{-19} cm^2 [29]) is expected. The π^*_2 resonances of the chloronitrobenzenes at about 0.2 eV, as well as the lowest-lying π^* resonance of benzene [25], are associated with $\ell = 3$ (f-wave), so that $\Delta E_{dps} \propto E^{3.5}$. As a result of its high-angular momentum term and much smaller VAEs, the π^*_2 resonance is expected to possess a mach larger survival probability than the σ^*_{C-Cl} resonance, thus favoring the DEA cross section through the occurrence of vibronic coupling and geometrical distortion of the anion state. The relative Cl^- yields from the $^2A_2$ π^*_2 and σ^*_{C-Cl} anion states of the chloronitrobenzenes can thus be traced back to their different lifetimes.

3.3. Low-resolution DEA spectra

The CEIYs of the studied nitrobenzenes recorded using the magnetic mass spectrometer with electron energy resolution of about 0.4 eV (FWHM) are shown in the bottom left panels of Figs. 1–8.

Because of convolution of the DEA cross sections with the energy distribution of the electron beam (see for instance chapter 4 and Fig. 6 of Ref. [30]), both the energy and relative heigths of corresponding DEA peaks are somewhat different in the high- and low-resolution DEA experiments (see Figs. 1–8). In addition, the two sets of data were obtained at significantly different temperatures (approximately 27 and 80 °C in the high- and low-resolution experiments, respectively). At least, a temperature

increase (vibrational excitation of the neutral molecules) leads to a shift of the peak maxima to lower energies and may influence the peak shape, mainly when the signal is due to unresolved contributions. The results of our low-resolution measurements for 1,2- and 1,3-nitrotoluene are in excellent agreement with the data of Ref. [16].

In addition to the negative species detected in the high-resolution DEA spectra (Table 2), the more sensitive low-resolution DEA apparatus allows detection of many low-intensity dissociation channels, leading to deep fragmentation of the parent anion, including ring cleavage and rearrangement processes. The peak energies and peak maximum relative intensities, which do not exceed 1.5%, are reported in Table 3, see columns 2 and 3. The weakness of these signals is in line with the complexity of the dissociation paths involved [31], the dominant dissociation channels (leading to NO_2^- and Cl^- formation) requiring only cleavage of a single bond. The occurrence of low-intensity rearrangement processes indicates that many internal degrees of freedom of the anion are excited and play a role in sharing the excess energy. Plausible schemes of the rearrangement dissociation processes observed in NIMS are shown below.

m/z 123 $(M\text{-}CH_2)^-$ from 1,2-nitrotoluene (3.6 eV) and 1,3-nitrotoluene (3.4 eV)

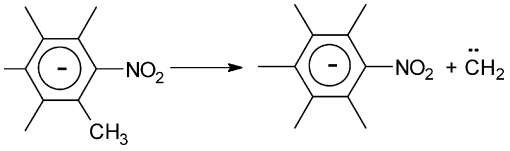

m/z 107 $(M\text{-}NO)^-$ from 1,2-nitrotoluene (3.6 eV) and 1,3-nitrotoluene (3.5 eV)

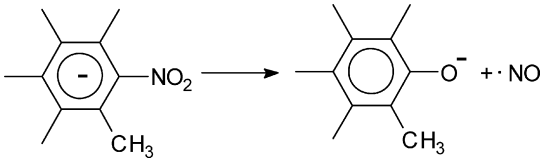

m/z 93 $(M\text{-}H_2\text{-}NO_2)^-$ from 1,2-fluoronitrobenzene (3.9 eV)

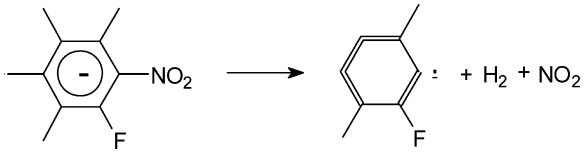

m/z 109 $(M\text{-}H_2\text{-}NO_2)^-$ from 1,3-chloronitrobenzene (4.0 eV)

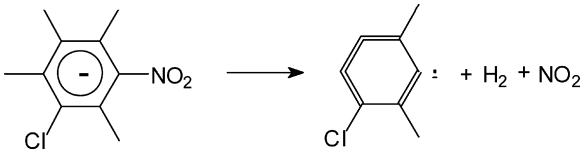

m/z 91 C_5HNO^- from 1,2-fluoronitrobenzene (3.6 eV), 1,3-fluoronitrobenzene (3.65 eV), 1,4-fluoronitrobenzene (3.7 eV)

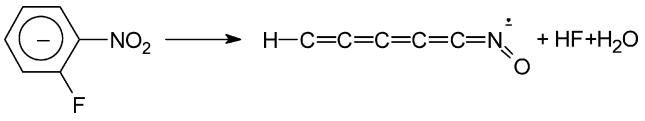

m/z 91 C_5HNO^- from 1,2-chloronitrobenzene (3.85 eV), 1,3- and 1,4-chloronitrobenzene (3.5 eV)

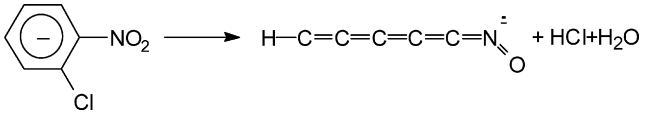

m/z 41 dipole bound state $C_2H_3N^-$ from 1,2-fluoronitrobenzene (4.1 eV), 1,3-fluoronitrobenzene (4.35 eV), and 1,4-fluoronitrobenzene (4.3 eV, 6.2 eV))

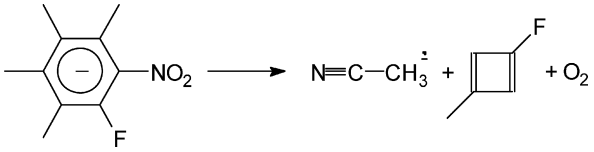

m/z 42 OCN^- from 1,4-fluoronitrobenzene (3.6 eV)

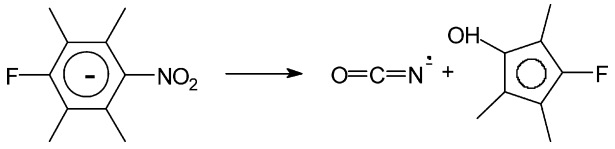

Table 3
MSNI data on halonitrobenzenes at the ion source temperature ~350 K

m/z	E_{max} (FWHM) (eV)	Relative intensity (% in parentheses)	Integral intensity including all, isotopes (%)	Structure
1,2-Nitrotoluene. τ_{AD}(0.02 eV) = 64 μs; τ_{AD}(0.0 eV) ~ 89 μs; T ~ 340 K				
137	**0.02 (0.36)**	**3631 (40.1)**	**20**	**M^-**
136	3.5 (1.0)	21 (0.2)		$(M-H)^-$
	7.0 (~1)	5.9 (0.07)		
123	0.0 (narrow)	0.8 (0.01)		$(M-CH_2)^-$
	3.6 (~1.3)	0.9 (0.01)		
121	4.3 (0.93)	39 (0.43)		$(M-O)^-$
107	1.0 (~0.7)	12.5 (0.14)		$(M-NO)^-$
	3.6 (1.22)	183 (2.0)		
46	**0.9 (0.88)**	**1850 (20.4)**	**21**	**NO_2^-**
	3.6 (1.28)	**3312 (36.6)**	**56**	
110.43	0.0	1.0 (0.01)	Very weak	$m^*_{137\rightarrow123}$
15.45	~0.0	0.6 (0.01)	Very weak	$m^*_{137\rightarrow46}$
1,3-Nitrotoluene. τ_{AD}(0.01 eV) = 68 μs; τ_{AD}(0.0 eV) ~95 μs; T ~ 340 K				
137	**0.01 (0.32)**	**6450 (59.7)**	**33**	**M^-**
136	3.6 (1.12)	45 (0.4)		$(M-H)^-$
	7.0 (1.3)	11 (0.1)		
123	3.4	1.2 (0.01)		$(M-CH_2)^-$ or $(M-N)^-$
121	4.3	28 (0.26)		$(M-O)^-$
107	3.5	187 (1.7)		$(M-NO)^-$
46	**0.54 (0.72)**	**560 (5.2)**	**5**	**NO_2^-**
	3.5 (1.15)	**3520 (32.6)**	**61**	
110.43	0.0 (1.1)	0.7 (0.006)	Very weak	$m^*_{137\rightarrow123}$
15.45	~0.0	0.6 (0.006)	Very weak	$m^*_{141\rightarrow46}$
1,2-Fluoronitrobenzene. τ_{AD}(0.01 eV) = 41 μs; τ_{AD}(0.0 eV) ~47 μs; T ~ 340 K				
141	**0.01 (0.35)**	**10,470 (20.3)**	**12.6**	**M^-**
111	0.51	1500 (2.9)		$(M-NO)^-$
95	3.5	275 (0.5)		$(M-NO_2)^-$
	4.6	253 (0.5)		
	6.6sh	70 (0.14)		
93	3.9	216 (0.4)		$(M-H_2-NO_2)^-$
91	3.6	740 (1.4)		C_5HNO^-
76	3.8	75 (0.15)		$C_6H_4^-$
75	4.1	210 (0.4)		$C_6H_3^-$
46	**0.54 (0.71)**	**33,278 (64.4)**	**72.5**	**NO_2^-**
	3.6 (1.2)	**3805 (7.4)**	**14.3**	
41	4.1	170 (0.3)		$C_2H_3N^-$
26	3.85	165 (0.3)		CN^-
19	3.8 (1.1)	176 (0.3)		F^-
16	4.4	276 (0.5)		O^-
15.01	~0.1	1.5 (0.003)	Very weak	$m^*_{141\rightarrow46}$
1,3-Fluoronitrobenzene. τ_{AD}(0.1 eV) = 67 μs; τ_{AD}(0.0 eV) ~129 μs; T ~ 340 K				
141	**0.1 ($0.64_{est.}$)**	**17,684 (29.9)**	**42.0**	**M^-**
	0.3 ($0.26_{est.}$)	**17,518 (30.0)**		
111	0.9	130 (0.2)		$(M-NO)^-$
	3.3	190 (0.3)		
91	3.65	173 (0.3)		C_5HNO^-
76	3.9	90 (0.15)		$C_6H_4^-$
46	**0.7 ($0.64_{est.}$)**	**8736 (14.8)**	**31.9**	**NO_2^-**
	1.1 ($0.52_{est.}$)	**8932 (15.1)**		
	3.4 (1.2)	**5488 (9.3)**	**26.0**	
41	4.35	29 (0.05)		$C_2H_3N^-$
26	4.0	40 (0.07)		CN^-
19	3.6 (1.1)	45 (0.08)		F^-
16	4.7	55 (0.09)		O^-
15.01	~0.3	12 (0.02)	Very weak	$m^*_{141\rightarrow46}$
1,4-Fluoronitrobenzene. τ_{AD}(0.07 eV) = 42 μs; τ_{AD}(0.0 eV) ~71 μs; T ~ 340 K				
141	**0.07 (0.42)**	**16,069 (74.0)**	**54.9**	**M^-**
140	3.1	15 (0.07)		$(M-H)^-$
125	0.1	3 (0.01)		$(M-O)^-$
	4.2	45 (0.2)		
124	3.8	60 (0.25)		$(M-OH)^-$

Table 3 (*Continued*)

m/z	E_{max} (FWHM) (eV)	Relative intensity (% in parentheses)	Integral intensity including all, isotopes (%)	Structure
111	1.0	10 (0.05)		$(M\text{-}NO)^-$
	3.3	140 (0.6)		
91	3.7	200 (0.9)		C_5HNO^-
76	3.7	37 (0.2)		$C_6H_4^-$
75	3.6	110 (0.5)		$C_6H_3^-$
46	**1.2 (0.52$_{est.}$)**	**1899 (8.7)**	**10.0**	**NO_2^-**
	3.6 (1.45)	**2966 (13.7)**	**35.0**	
42	3.6	25 (0.1)		OCN^-
41	4.3	25 (0.1)		$C_2H_3N^-$
	6.2	10 (0.05)		
26	3.9	54 (0.25)		CN^-
19	4.0 (1.35)	7.4 (0.03)	0.1	F^-
16	4.4	41 (0.2)		O^-
15.01	∼0.03	2.3 (0.01)	Very weak	$m^*_{141\rightarrow46}$
1,2-Chloronitrobenzene. τ_{AD}(0.05 eV) = 32 μs; τ_{AD}(0.0 eV) ∼51 μs; T ∼ 340 K				
157	**0.05 (0.41)**	**8045 (24.0)**	**20.7**	**M^-**
141	4.2	16.6 (0.05)		$(M\text{-}O)^-$
127	0.0sh	80 (0.2)		$(M\text{-}NO)^-$
	0.65	166 (0.5)		
111	4.75	17.0 (0.05)		$(M\text{-}NO_2)^-$
109	4.1	15.4 (0.05)		$(M\text{-}H_2\text{-}NO_2)^-$
91	3.85	28.5 (0.85)		C_5HNO^-
46	**0.5 (0.66)**	**5906 (17.6)**	**17.0**	**NO_2^-**
	3.5 (0.99)	**1269 (3.8)**	**5.4**	
35	**0.3 (0.52)**	**17,604 (52.6)**	**56.0**	**Cl^-**
	3.6 (0.54)	**293 (0.9)**	**0.9**	
26	3.9	7.3 (0.02)		CN^-
16	4.5	8.6 (0.03)		O^-
13.48	∼0.1	0.3 (0.0009)	Very weak	$m^*_{157\rightarrow46}$
7.8	∼0.2	8.5 (0.03)	Very weak	$m^*_{157\rightarrow35}$
1,3-Chloronitrobenzene. τ_{AD}(0.1 eV) = 65 μs; τ_{AD}(0.0 eV) ∼115 μs; T ∼ 340 K				
157	**0.1 (0.41)**	**51,333 (80.8)**	**74.7**	**M^-**
141	0.2	5 (0.008)		$(M\text{-}O)^-$
	4.2	52.5 (0.08)		
140	3.3	15 (0.02)		$(M\text{-}OH)^-$
127	0.7	134 (0.2)		$(M\text{-}NO)^-$
	2.8	15 (0.02)		
109	4.0	16 (0.02)		$(M\text{-}H_2\text{-}NO_2)^-$
92	4.15	14 (0.02)		$C_5H_2NO^-$
	6.2	8.7 (0.01)		
91	3.5	51 (0.08)		C_5HNO^-
76	3.7	12.9 (0.02)		$C_6H_4^-$
75	3.6	12.7 (0.02)		$C_6H_3^-$
46	**1.0 (0.66)**	**2823 (4.4)**	**4.4**	**NO_2^-**
	3.3 (1.23)	**2756 (4.3)**	**8.3**	
41	3.7	13.5 (0.02)		$C_2H_3N^-$
35	**0.4 (0.58)**	**2681 (4.2)**	**8.0**	**Cl^-**
	0.8 (0.7)	**2417 (3.8)**		
	3.3 (1.34)	**1140 (1.8)**	**4.7**	
16	4.5	21 (0.03)		O^-
13.48	∼0.1	2.0 (0.003)	Very weak	$m^*_{157\rightarrow46}$
7.8	∼0.2	5.2 (0.008)	Very weak	$m^*_{157\rightarrow35}$
1,4-Chloronitrobenzene. τ_{AD}(0.07 eV) = 59 μs; τ_{AD}(0.0 eV) ∼111 μs; T ∼ 340 K				
157	**0.07 (0.44)**	**28,270 (59.1)**	**61.2**	**M^-**
156	0.0	Very weak		$(M\text{-}H)^-$
	3.2	20 (0.04)		
141	4.15	124 (0.26)		$(M\text{-}O)^-$
140	3.25	26 (0.05)		$(M\text{-}OH)^-$
127	0.8	84 (0.18)		$(M\text{-}NO)^-$
	2.9	52 (0.1)		
126	3.9	23 (0.05)		$(M\text{-}HNO)^-$
122	4.1	30 (0.06)		$(M\text{-}Cl)^-$
	6.1	15 (0.03)		

Table 3 (*Continued*)

m/z	E_{max} (FWHM) (eV)	Relative intensity (% in parentheses)	Integral intensity including all, isotopes (%)	Structure
91	3.5	184 (0.38)		C_5HNO^-
76	3.7	40 (0.08)		$C_6H_4^-$
75	3.55	70 (0.15)		$C_6H_3^-$
42	3.4	37 (0.08)		OCN^-
46	**0.9 (0.75)**	**2731 (5.71)**	**5.0**	**NO_2^-**
	3.4 (1.27)	**6993 (14.6)**	**12.5**	
35	**0.5_{sh} ($0.64_{est.}$)**	**4917 (10.3)**	**14.6**	**Cl^-**
	0.7_{sh} ($0.69_{est.}$)	**2894 (6.0)**		
	3.4 (1.3)	**1183 (2.5)**	**6.7**	
26	4.0	35 (0.07)		CN^-
16	4.3	85 (0.18)		O^-
13.48	∼0.1	1.0 (0.002)	Very weak	$m^*_{157\rightarrow46}$
7.8	∼0.2	3.0 (0.006)	Very weak	$m^*_{157\rightarrow35}$

Mean autodetachment lifetime τ_{AD} for the maximum of the NI peak. Main dissociation channels are marked by bold face.

Table 3 and Figs. 1–8 (bottom right panels) report the measured mean autodetachment lifetimes of the molecular NIs. The present results are in reasonable agreement with previously published data [14]. The lifetimes ($\tau_{AD}(E_{max})$) given in Table 3 refer to the maximum of the M^- peak (given in parentheses). Estimated zero electron energy lifetimes ($\tau_{AD}(0)$) are also listed. As shown by Christophorou et al. [12–14] the lifetime decreases exponentially with increasing energy. So, comparison of the lifetimes extrapolated to zero energy seems to be more correct. A crude estimate (see Eq. (5)) of the lifetimes at zero energy can be obtained from the theoretical curves shown in the bottom right panels of Figs. 1–8.

In addition to the above-mentioned low-intensity NIs, metastable anions (with respect to dissociation [17,31]) have been detected in all the studied nitrobenzenes. The intensity of these signals, observed only at incident electron energies close to zero, is always very small, see Table 3. In the chloronitrobenzenes, metastable NIs were found at *m/z* 7.8 a.m.u., corresponding to the $M^{-*} \rightarrow Cl^- + (M - Cl^-)$ decay process, and *m/z* 13.5 a.m.u., corresponding to the $M^{-*} \rightarrow NO_2^- + (M - NO_2)$ decay process. Metastable elimination of NO_2^- from the parent molecular anions of the fluorine and methyl derivatives was detected at *m/z* 15.0 and 15.4 a.m.u., respectively. Repeated measurements have shown that the abundance of both the parent and metastable ions increases linearly with the sample pressure, thus indicating that the role played by collision induced fragmentation is not significant.

Metastable ions are formed outside the ion source, in the acceleration region or even in the first field-free drift region of the magnetic mass spectrometer. The corresponding broad spectral features are centered at an apparent mass (m^*) given by the approximate formula $m^* = m^2/M$ [17], where m and M are the masses of the daughter and parent ions, respectively. Usually, the incident electron energy required for formation of metastable ions is intermediate between those required for the parent and daughter ions. However, the energy also depends on the particular instrumental geometry (time of anion extraction from the ion source) and voltage settings used in each experiment. Of course, it also depends on the decay rate of the parent ion. In any case, a requirement for observation of metastable NIs in a magnetic mass spectrometer is that the decay processes take place on the time scale of microseconds [17].

3.4. Discussion of anion decay kinetics

Curves of effective yield of metastable anions are shown in the higher right panels of Figs. 1–8. In 1,2-fluoronitrobenzene metastable ions are observed up to 0.44 eV; in 1,3-fluoronitrobenzene this border is located at ∼0.7 eV, in 1,2-chloronitrobenze at 0.4 eV, in 1,3-chloronitrobenzene and 1,4-chloronitrobenzene at 0.55 eV. These experimental findings demonstrate that anion fragmentation is very slow. At low energies (the exact upper limit also depends upon the particular instrumental conditions) it is thus possible to describe these processes in the framework of a statistical approximation [32–34]. NIs which dissociate inside the ion source, but after a time much longer than a nuclear vibrational period, are detected as "normal" species. If the resolution of the mass filter is sufficiently high, broadening of the corresponding signals can be observed. However, even in this case the dissociation process can still be described in a statistical approximation.

Willey et al. [34] analyzed the temperature dependence of the $[Cl^-]/[M^-]$ intensity ratio for thermal electron attachment to C_2Cl_3H and C_2Cl_4 using chemical ionization mass spectrometry. Two distinct slopes were observed in the plot of $\ln([Cl^-]/[M^-])$ as an inverse function of temperature. Using these data, the difference in activation energies for the formation of the ground anion state and the next excited anion state, as well as the detachment energy of the ground anion state, i.e., the adiabatic electron affinity, may be obtained.

Also for the present substituted nitrobenzenes, where long-lived parent anions and metastable anions corresponding to the dominant fragments can be observed, it should thus be possible to describe the processes of autodetachment of captured electrons and dissociation of the parent molecular anions in terms of kinetic equilibrium. For the reaction $AB + e^- \underset{k_{-1}}{\overset{k_1}{\Leftrightarrow}} AB^- \xrightarrow{k_2} A + B^-$, where AB represents the target molecule, k_1, k_{-1} and k_2 are the rate constants for electron attachment, detachment, and dissociation, respectively, the following kinetic equations for the

Table 4
Parameters set for kinetic calculations

Compound	P_a	$P_d(NO_2)$	$P_d(Cl)$	DE(C-NO_2) (eV)	DE(C-Cl) (eV)
1,2-Nitrotoluene	0.5×10^{-4}	1.5×10^{-2}	–	1.45	–
1,3-Nitrotoluene	0.85×10^{-4}	1.5×10^{-2}	–	1.45	–
1,2-Fluoronitrobenzene	2×10^{-4}	1.75×10^{-2}	–	1.45	–
1,3-Fluoronitrobenzene	5×10^{-4}	2×10^{-3}	–	1.45	–
1,4-Fluoronitrobenzene	1.8×10^{-4}	2×10^{-3}	–	1.45	–
1,2-Chloronitrobenzene	6×10^{-4}	6.5×10^{-3}	1.3×10^{-3}	1.45	1.1
1,3-Chloronitrobenzene	6×10^{-4}	1×10^{-3}	2×10^{-4}	1.45	1.1
1,4-Chloronitrobenzene	4×10^{-4}	8×10^{-4}	1.5×10^{-4}	1.45	1.1

P_a is the autodetachment probability; $P_d(NO_2)$ and $P_d(Cl)$ are the dissociation probabilities for appropriate dissociative pathway. DE means dissociation energies of the C–N and C–Cl bonds.

ion intensities may be written

$$[AB^-] = [AB_0^-] \exp[-(k_{-1} + k_2)t], \quad (2)$$

$$[B^-] = \frac{[AB_0^-]k_2}{k_{-1} + k_2}(1 - \exp[(k_{-1} + k_2)t]), \quad (3)$$

where $[AB_0^-]$ = const is the intensity of molecular anion at $t = 0$, t is detection time. The rate constants k_{-1} and k_2 depend on electron energy (E) and temperature (T) of the target molecule. The total vibrational energy of the neutral target molecule as a function of temperature may be expressed as [35]

$$E_{vib} = \sum_{k=1}^{N} \frac{\omega_k}{\exp(\omega_k/kT) - 1}, \quad (4)$$

where $N = 3n - 6$ is the number of vibrational degrees of freedom, ω_k are vibrational frequencies obtained from semiempirical quantum chemical PM3 calculations. We use the same formula to evaluate the anion vibrational energy storage [35]. Then, the rate constants for autodetachment and dissociation are

$$k_{-1} = \frac{P_a \exp(-\hbar\omega_a/kT)}{t_a Z}, \qquad k_2 = \frac{P_d \exp(-\hbar\omega_d/kT)}{t_d Z}, \quad (5)$$

where P_a and P_d are probabilities of autodetachment and dissociation, respectively, t_a and t_d the typical vibrational periods for the autodetachment and dissociation potential curves, $\hbar\omega_a$ and $\hbar\omega_d$ the corresponding vibrational frequencies and Z is the statistical sum. Generally several anion vibrational modes may participate into a given dissociation or autodetachment process, so that expressions (5) may be a sum [36]. The total vibrational energy stored in the anion is

$$E_{total} = E + EA + E_{vib}, \quad (6)$$

where E is the incident electron energy and EA the adiabatic electron affinity of the target molecule. Substitution of (4), (5), and (6) into (2) and (3) leads to the typical behaviour of the relationship $\ln([B^-]/[AB^-])$ as a function of E, so-called decay curve. The results of calculation together with the experimental curves are shown in the right middle panels of Figs. 1–8.

The value of P_a may be evaluated from the experimental autodetachment lifetime. P_d values depend on the intensity of the dissociation channels observed in the experiment, and may be, in principle, estimated from the curves of NI effective yield. However the last quantity is a function of the (unknown) absolute electron capture cross section. A possible way (which does not require knowledge of the absolute capture cross section) for evaluating P_d values takes advantage of the energy dependence of $\ln([B^-]/[AB^-])$ [34]. In fact, the ratio $[B^-]/[AB^-]$ (see Eqs. (2) and (3) is independent from $[AB_0^-]$. Evaluation of the P_d parameters was performed by using the curves displayed in the middle right panels of Figs. 1–8. The values of P_a, P_d and dissociation energies using in calculations are listed in Table 4.

The same result may be reached by consideration of the so called decay curves, as commonly used in positive ion mass spectrometry [34]:

$$\frac{[AB^-]}{[AB^-] + [B^-]}, \qquad \frac{[B^-]}{[AB^-] + [B^-]}.$$

Here $[AB^-] + [B^-]$ is the total ion current. Both of these approaches, daughter/parent ion intensity ratio and decay curves analysis, do not consider the electron attachment cross section, but only the kinetics of the anion decay.

In the case of 1,3-, 1-4-fluoronitrobenzenes and chloronitrobenzenes the shape resonance associated with occupation of the π_2^* MO lies in an electron energy range corresponding to the "slow decay". Thus for these compounds the following scheme may be applied

$$M + e^- \xrightarrow{\text{capture}} M_2^- \xrightarrow{\text{electron relaxation}} M_1^{-*} \xrightarrow{\text{dissociation}} (M\text{–}R)^\bullet + R^-,$$

where M_2^- represents the π_2^* anion state and M_1^* the vibrationally excited first anion state. However, in a better approximation temperature effects should also be considered. For instance, vibrational energy storage of the anion increases with temperature, whereas the autodetachment lifetime decreases. Moreover, dissociation is also a temperature dependent process, see Eq. (5).

The differences between the present high- and low-resolution spectra are pronounced in the low-energy region of the spectra of 1,3-fluoronitrobenzene and the chloronitrobenzenes, while at high-electron energies they become smaller, except for 1,2- and 1,3-nitrotoluene. In particular, the shape of the M^- current in 1,3-fluoronitrobenzene recorded with the two experiments is notably different (see Fig. 4, central and bottom panels). The peak at lowest energy (0.02 eV) is about 15 times more

intense than the second peak (0.23 eV) using the high-resolution spectrometer. In contrast, the intensities of the corresponding peaks recorded using the low-resolution spectrometer are nearly equal. Taking into account that the autodetachment lifetime for the parent negative ion is of the order of microseconds, this difference may be explained in terms of the different time required for ion detection in the two instruments. The flight time of the molecular ion of 1,3-fluoronitrobenzene (m/z 141 a.m.u.) is evaluated to be about $t_f \sim 130\,\mu s$ in our high-resolution DEA experiments. The estimated flight time of this anion through the magnetic mass filter is $t_f \sim 20$–$25\,\mu s$ in the low-resolution DEA apparatus. According to our measurements, the autodetachment lifetime of 1,3-fluoronitrobenzene decreases exponentially with the incident electron energy: $\tau_{AD} \sim 67\,\mu s$ at 0.1 eV, $\tau_{AD} \sim 38\,\mu s$ at 0.23 eV and $\tau_{AD} \sim 33\,\mu s$ at 0.3 eV, in good agreement with earlier data [13,14]. Therefore, the lifetime of the parent anion of 1,3-fluoronitrobenzene at 0.02 eV may be evaluated as $\tau_{AD} \sim 100\,\mu s$. Assuming that the flight time of the parent anion of 1,3-fluoronitrobenzene is 100 μs, the relationship of the intensities at 0.02 and 0.23 eV will be $\exp[-\tau_{AD}(0.02)/t_f]/\exp[-\tau_{AD}(0.23)/t_f] \sim 0.37/0.07$ in the high-resolution DEA experiment. The same relationship in the low-resolution DEA apparatus for intensities at 0.1 and 0.3 eV is 0.74/0.55. These estimates reproduce satisfactorily the observed results for the parent anion of 1,3-fluoronitrobenzene. In a better approximation, the energy spread of the incident electron beam (which strongly influences the observed magnitude of sharp peaks) and the temperature of the target molecule (which influences the autodetachment lifetime of the parent anions) should also be taken into account.

Thus, the differences between the present high- and low-resolution DEA results, summarized in Table 2, likely arise from four factors: (i) different incident electron energy resolutions, (ii) different time scales, (iii) different temperatures and (iv) possible different ionization efficiencies at low- and high-electron energy for the high- and low-resolution ion sources. The high-resolution DEA spectrometer provides a more correct profile of the DEA cross section as a function of incident electron energy. Whereas the intensity of broad features is only slightly affected by the electron energy resolution, sharp features are smeared and their heights decrease in the low-resolution DEA spectra. The relative intensities of fragment ions in low-resolution spectra are systematically sizeably lager, see Tables 2 and 3. Obviously, this is a result of the second or/and fourth factors.

4. Conclusion

A series of nitrobenzene derivatives (methyl, fluoro and chloro substituted) was investigated by means of the ETS, DEAS, and NIMS techniques. The energies of vertical electron attachment measured in the ET spectra are satisfactorily reproduced by scaling with appropriate empirical equations the neutral state virtual orbital energies supplied by HF/6-31G and B3LYP/6-31G* calculations. The same approach also predicts the first vertical anion state of each compound to be stable (thus not observable in ETS). The evaluated vertical EAs are fully consistent (0.3 eV smaller) with the experimental adiabatic EAs (associated with formation of the anion in its optimized geometry) reported in the literature.

The maxima displayed by the negative currents (essentially due to the molecular anion and the NO_2^- and Cl^- fragments) measured in the DEA spectra can be correlated with corresponding features of the ET spectra. Competition between autodetachment and dissociation controls the shape of the DEA cross sections. All investigated molecules form long-lived molecular NIs. The DEA data allow to evaluate the average values of autodetachment life-time of the molecular anions. For the sake of direct comparison, these autodetachment lifetimes have been extrapolated to zero electron energy.

The presence of metastable anions associated with Cl^- and NO_2^- production indicates directly that these dissociation channels take place in the time scale of microseconds at low-electron energy. Analysis of the decay curves and comparison with model kinetic calculations indicate that the second π* anion state (slightly unstable and with mainly benzene character) of the 1,3- and 1,4-fluoro and chloronitrobenzenes can dissociate through the intermediate ground electronic state.

Acknowledgements

This work was financially supported by the Russian Foundation for Basic Research, Grant #06-03-32059-a, by the Slovak Science and Technology Assistance Agency under the contract No. APVT-20-007504, and by the Italian Ministero dell'Istruzione, dell'Università e della Ricerca.

References

[1] L. Sanche, G.J. Schulz, J. Phys. Rev. A 5 (1972) 1672.
[2] G.J. Schulz, Rev. Mod. Phys. 45 (1973) 423.
[3] K.D. Jordan, P.D. Burrow, Acc. Chem. Res. 11 (1978) 341.
[4] H.A. Jiménez-Vázquez, M.E. Ochoa, G. Zepeda, A. Modelli, D. Jones, J.A. Mendoza, J. Tamariz, J. Phys. Chem. A 101 (1997) 10082.
[5] A. Modelli, M. Venuti, Int. J. Mass Spectrom. 205 (2001) 7.
[6] S.W. Staley, J.T. Strnad, J. Phys. Chem. 98 (1994) 116.
[7] A. Modelli, Phys. Chem. Chem. Phys. 5 (2003) 2923.
[8] A. Modelli, B. Hajgató, J.F. Nixon, L. Nyulászi, J. Phys. Chem. A 108 (2004) 7440.
[9] D.A. Chen, G.A. Gallup, J. Chem. Phys. 93 (1990) 8893.
[10] G. Gallup, K. Aflatooni, P.D. Burrow, J. Chem. Phys. 118 (2003) 2562.
[11] T.F. O'Malley, Phys. Rev. 150 (1966) 14.
[12] L.G. Christophorou, A. Hadjiantoniu, J.G. Carter, J. Chem. Soc., Faraday Trans. II 69 (1973) 1713.
[13] J.P. Johnson, D.L. McCorkle, L.G. Christophorou, J.G. Carter, J. Chem. Soc., Faraday Trans. II 71 (1975) 1742.
[14] L.G. Christophorou, M.W. Grant, D.L. McCorkle, Adv. Chem. Phys. 36 (1977) 413.
[15] L.G. Christophorou, K.S. Gant, V.E. Anderson, J. Chem. Soc., Faraday Trans. II 73 (1977) 804.
[16] C.D. Harvey, M. Eberhart, T. Jones, K.J. Voorhees, J.A. Laramée, R.B. Cody, D.P. Clougherty, J. Phys. Chem. A 110 (2006) 3313.
[17] J.H. Beynon, Mass Spectrometry and its Applications to Organic Chemistry, Elsevier Publishing Co., Amsterdam, 1960.
[18] A. Modelli, D. Jones, G. Distefano, Chem. Phys. Lett. 86 (1982) 434.
[19] R. Johnston, P.D. Burrow, J. Electron Spectrosc. Relat. Phenom. 25 (1982) 119.
[20] Š. Matejčik, V. Foltin, M. Stano, J.D. Skalný, Int. J. Mass Spectrom. 223/224 (2003) 9.

[21] M.J. Frisch, G.W. Trucks, H.B. Schlegel, G.E. Scuseria, M.A. Robb, J.R. Cheeseman, V.G. Zakrzewski, J.A. Montgomery Jr., R.E. Stratmann, J.C. Burant, S. Dapprich, J.M. Millam, A.D. Daniels, K.N. Kudin, M.C. Strain, O. Farkas, J. Tomasi, V. Barone, M. Cossi, R. Cammi, B. Mennucci, C. Pomelli, C. Adamo, S. Clifford, J. Ochterski, G.A. Petersson, P.Y. Ayala, Q. Cui, K. Morokuma, D.K. Malick, A.D. Rabuck, K. Raghavachari, J.B. Foresman, J. Cioslowski, J.V. Ortiz, B.B. Stefanov, G. Liu, A. Liashenko, P. Piskorz, I. Komaromi, R. Gomperts, R.L. Martin, D.J. Fox, T. Keith, M.A. Al-Laham, C.Y. Peng, A. Nanayakkara, C. Gonzalez, M. Challacombe, P.M.W. Gill, B. Johnson, W. Chen, M.W. Wong, J.L. Andres, C. Gonzalez, M. Head-Gordon, E.S. Replogle, J.A. Pople, Gaussian 98, Revision A.6, Gaussian Inc., Pittsburgh, PA, 1998.
[22] S. Chowdhury, T. Heinis, E.P. Grimsrud, P. Kebarle, J. Phys. Chem. 90 (1986) 2747.
[23] A. Modelli, Trends Chem. Phys. (Res. Trends) 6 (1997) 57.
[24] P.D. Burrow, A. Modelli, K.D. Jordan, Chem. Phys. Lett. 132 (1986) 441.
[25] D.D. Clarke, C.A. Coulson, J. Chem. Soc. A 1 (1969) 169.
[26] A. Modelli, M. Venuti, J. Phys. Chem. A 105 (2001) 5836.
[27] K. Aflatooni, P.D. Burrow, J. Chem. Phys. 113 (2000) 1455.
[28] E.P. Wigner, Phys. Rev. 73 (1948) 1002.
[29] D.M. Pearl, P.D. Burrow, J. Chem. Phys. 101 (1994) 2940.
[30] M.-W. Ruf, S. Barsotti, M. Braun, H. Hotop, I.I. Fabrikant, J. Phys. B: At. Mol. Opt. Phys. 37 (2004) 41.
[31] V.I. Khvostenko, S.R. Rafikov, Doklady AN SSSR (Rus.) 220 (1975) 892.
[32] B.L. Donnally, H.E. Carr, Phys. Rev. 93 (1) (1954) 111.
[33] J.A. Hipple, R.E. Fox, E.U. Condon, Phys. Rev. 69 (7/8) (1946) 347.
[34] J.R. Willey, E.C. Chen, W.E. Wentworth, J. Phys. Chem. 97 (1993) 1256.
[35] Š. Matejčik, T.D. Märk, P. Spanel, D. Smith, T. Jaffke, E. Illenberger, J. Chem. Phys. 102 (1995) 2516.
[36] E.E. Nikitin, Theory of Elementary Atomic-Molecular Processes in Gas Phase, Khimia, Moscow, 1970.